

The Millennium Galaxy Catalogue: Star counts and the Structure of the Galactic Stellar Halo

D.J. Lemon^{1,2*}, Rosemary F. G. Wyse^{1,3,4}, J. Liske⁵, S.P. Driver² and Keith Horne¹

¹*School of Physics and Astronomy, University of St Andrews, North Haugh, St Andrews, Fife, KY16 9SS, UK*

²*Research School of Astronomy and Astrophysics, Mount Stromlo Observatory, Cotter Road, Weston, ACT 2611, Australia*

³*Astrophysics, Oxford University, Oxford, UK*

⁴*Physics & Astronomy Dept., The Johns Hopkins University, Baltimore, MD 21218, USA (permanent address)*

⁵*Institute for Astronomy, University for Edinburgh, Royal Observatory, Blackford Hill, Edinburgh, EH9 3HJ.*

Accepted Received

ABSTRACT

We derive a star catalogue generated from the images taken as part of the $\sim 37.5 \text{ deg}^2$ Millennium Galaxy Catalogue. These data, alone and together with colours gained from the Sloan Digital Sky Survey Early Data Release, allow the analysis of faint star counts ($B_{\text{MGC}} < 20$) at high Galactic latitude ($41^\circ < b < 63^\circ$), as a function of Galactic longitude ($239^\circ < l < 353^\circ$). We focus here on the inner stellar halo, providing robust limits on the amplitude of substructure and on the large-scale flattening. In line with previous results, the thick disk, an old, intermediate-metallicity population, is clearly seen in the colour-magnitude diagram. We find that the Galactic stellar halo within $\sim 10 \text{ kpc}$ (the bulk of the stellar mass) is significantly flattened, with an axial ratio of $(c/a) = 0.56 \pm 0.01$, again consistent with previous results. Our analysis using counts-in-cells, angular correlation functions and the Lee 2D statistic, confirms tidal debris from the Sagittarius dwarf but finds little evidence for other substructure in the inner halo, at heliocentric distances of $\lesssim 5 \text{ kpc}$. This new quantification of the smoothness in coordinate space limits the contribution of recent accretion/disruption to the build-up of the bulk of the stellar halo.

Key words: astronomical data bases: catalogues – galaxy: structure – galaxies: halo

1 INTRODUCTION

The basic stellar components of the Milky Way are the thin disk, thick disk, stellar halo and central bulge, albeit that the inter-relationships and distinction amongst different components remains subject to some debate (e.g. Norris & Ryan 1991). Quantifying the properties of the stellar components of the Milky Way Galaxy is of wide importance, since the multi-variate stellar distribution function is a product of Galaxy formation and evolution and in turn constrains those processes that are important during and after the formation of the stars. The thick disk of the Milky Way galaxy was introduced by Gilmore & Reid (1983) based on their deep star counts towards the South Galactic Pole that were best fit by including a component with a scale-height some 3–4 times that of the old thin disk; this component has the characteristics of ‘Intermediate Population II’ (Oort 1958) and is clearly seen in earlier star counts (Elvius 1965; Weistrop 1972; Yoshii 1982). That the stellar population of

the thick disk is distinct from that of the halo is seen clearly in colour magnitude diagrams derived from star count surveys (e.g. Fig. 2 of Gilmore, Wyse & Kuijken 1989; Chen et al. 2001; Fig. 4 here), and many derivations of the field kinematics and metallicity distributions have established its existence definitively.

However, even the structural parameters of these major stellar components of the Galaxy are less well-established, and deep wide-area star counts are important in their determination. The flattening of the stellar halo, when combined with metallicity and kinematic information, can distinguish between models in which the halo formed with a little, or with a lot, of gaseous dissipation, and constrains the flattening of the dark matter halo (e.g. White 1985). Substructure in phase space is expected in hierarchical clustering theories of Galaxy formation, and while the signature in kinematics may be more obvious and long-lived (e.g. Helmi & White 1999; Helmi et al. 1999), late accretion and merging may produce observable over-densities in coordinate space (e.g. Johnston, Hernquist & Bolte 1996; Zhang et al. 2002). The streams from the Sagittarius dwarf spheroidal galaxy

* E-mail: djl6@st-andrews.ac.uk

are extreme examples (e.g. Yanny et al. 2000; Ibata et al. 2001; Vivas et al. 2001; Ibata et al. 2002). Placing constraints on the level of clustering in coordinate space, for the bulk of the stellar halo, is obviously important to constrain recent tidal disruption of, and accretion of stars from, satellite stellar systems.

Most previous investigations have utilised small area star counts in a few selected lines-of-sight (e.g. Gilmore & Reid 1983; Bahcall & Soneira 1984; Wyse & Gilmore 1989; Reid & Majewski 1993). Investigations into large-scale Galactic structure, and to quantify the global importance of potentially rare effects – such as substructure – obviously benefit from large-area surveys. While combination of the data-sets from several independent smaller surveys is possible (cf. Reylé & Robin 2001), the advantages of uniformity of photometry, star-galaxy classification etc. all argue for the superiority of one survey across a wide range of Galactic coordinates. This has recently become possible through the advent of wide-field CCD mosaic cameras on medium-sized telescopes, such as that built for the Sloan Digital Sky Survey (York et al. 2000) and the Wide Field Camera (WFC) on the Isaac Newton 2.5m Telescope (INT).

In this paper we derive a star catalogue generated from images taken with the INT/WFC for the ~ 37.5 deg² Millennium Galaxy Catalogue (MGC; Liske et al. 2003). From this catalogue, and in conjunction with colours gained from the Sloan Digital Sky Survey Early Data Release (SDSS-EDR; Stoughton et al. 2002), we obtain reliable star counts, to a limiting magnitude of $B_{\text{MGC}} = 20$ mag, as a function of Galactic longitude. The survey is exclusively at high Galactic latitudes, $b > 40^\circ$, and we investigate the structure of the Galactic stellar halo, with an emphasis on its flattening and on the quantification of the statistical significance of (or lack of) substructure.

This paper is divided into 5 sections. In Section 2 we describe the data used in this investigation. In Section 3 and Section 4 we describe the modeled and observed star counts respectively. The conclusions are presented in Section 5.

2 THE DATA

Our star catalogue is derived from the imaging survey designed to provide the Millennium Galaxy Catalogue (MGC; described in detail in Liske et al. 2003). This consists of a 37.5 deg² single-band deep ($\mu_{\text{lim}} = 26$ mags arcsec⁻²) survey along the equatorial strip, and overlaps in sky coverage with both the Two Degree Field Galaxy Redshift Survey (2dFGRS; Colless et al. 2001), and the Sloan Digital Sky Survey Early Data Release (SDSS-EDR; Stoughton et al. 2002). All 144 data frames were taken using the Wide Field Camera on the 2.5m Isaac Newton Telescope situated at La Palma. The WFC is a prime-focus instrument, and is a mosaic of four 4k×2k thinned EEV CCDs for the science data, with a smaller 2k×2k Loral CCD used for auto-guiding. The science CCDs have a pixel scale of 0.333 arcsec pixel⁻¹, and the layout gives a total sky coverage of 0.29 deg² per pointing. Each pointing was observed for a single 750 s exposure through a Kitt Peak National Observatory *B* filter (B_{KPNO}). Pointing 1 (field 1) is centered on RA = 10^h00^m00^s, DEC = 00°00′00″ (J2000) and pointing 144 (field 144) is centered on RA = 14^h46^m00^s,

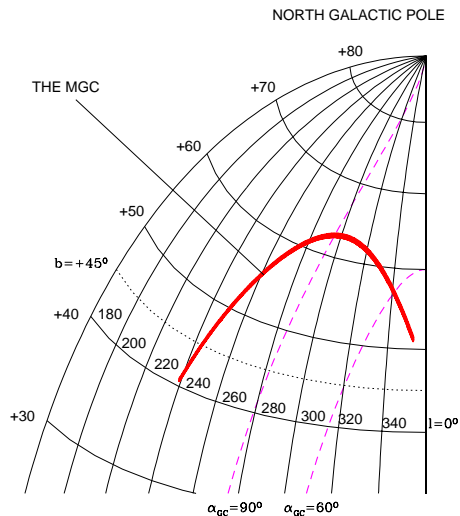


Figure 1. An Aitoff projection of the MGC strip. The small-dashed line marks the $b > 45^\circ$ cut. α_{GC} is the contour of constant angle from the Galactic center. The long-dashed lines at $\alpha_{\text{GC}} = 90^\circ$ and 60° indicate the points at b_{max} and $l=340^\circ$ respectively.

DEC = 00°00′00″ (J2000); Fig. 1 displays the MGC strip as an Aitoff projection in Galactic coordinates; note the emphasis on high Galactic latitudes.

The MGC astrometry is accurate to ± 0.08 arcsec in both RA and DEC, and the photometry is internally consistent to < 0.03 mag (see Liske et al. 2003). Star-galaxy classification is based on the ‘stellaricity’ parameter produced by the SExtractor software package, determined for each object using an artificial neural network that was trained extensively to differentiate between stars and galaxies (see Bertin & Arnouts 1996 for details). All cosmic rays, CCD defects, satellite trails, diffraction spikes and asteroids have been masked and removed from the catalogue. As shown in Liske et al. (2003), star-galaxy separation is extremely reliable for $16 < B_{\text{MGC}} < 20$; the star-count investigation in this paper is thus limited to this magnitude range¹ (the MGC-BRIGHT catalogue) giving us a total sample of 42413 stars.

The basic star catalogue is thus based on *B*-band magnitudes. We first investigate Galactic structure using these single-band data alone. We then exploit the overlap with the SDSS Early Data Release to isolate F-stars, thus targeting the turn-off of the stellar halo.

3 STAR COUNT MODEL

The star count model we use is that developed by Gilmore (1984; see also Gilmore, Reid & Hewett 1985 and Wyse & Gilmore 1989) and includes a double-exponential thin disk,

¹ Note that the MGC is complete down to $B_{\text{MGC}}=23.5$ mag and detects point sources to $B_{\text{MGC}} \approx 25$ mag, but accurate star-galaxy separation is limited to an imposed cut at $B_{\text{MGC}}=20$ mag.

a double-exponential thick disk, and a de Vaucouleurs stellar halo. The thin disk and halo luminosity functions are based on those of Wielen (1974). For the thick disk the Wielen LF applies only for $M_V > 4.5$ – for $M_V < 4.5$ the luminosity function of the thick disk follows that of 47 Tuc, the globular cluster with metallicity and age similar to that of a typical thick disk star (cf. Gilmore, Wyse & Jones 1995). Indeed the colour-magnitude relation of 47 Tuc is adopted for the thick disk. The colour-magnitude relation of the metal-poor globular cluster M5 is adopted for the stellar halo.

To facilitate our determination of the flattening of the stellar halo we held all the structural parameters of this model fixed, with the exception of the stellar halo axial ratio. We adopted a solar Galactocentric distance of 8 kpc, an old thin disk scale-height of 325 pc, a thin (and thick) disk scale length of 3.5 kpc, a thick disk scale-height of 1300 pc and thick-disk normalisation in the mid-plane, relative to the thin disk, of 2 per cent. The major-axis de Vaucouleurs radius for the stellar halo was fixed at 2700 pc. We made predictions for models with oblate stellar halos, with axial ratio (c/a) in the range 0.45 - 0.80, at a resolution of 0.01, and all with a local normalisation of the stellar halo relative to the thin disk of 0.125 per cent (cf. Morrison 1993).

With these parameter values, the stellar halo does not contribute significantly to the star counts until $B \gtrsim 17.5$ mag (shown graphically in Fig. 4 below). Given our intended aim here is to investigate the structure of the halo, we will only compare with data fainter than this limit.

4 THE OBSERVED STAR COUNTS

4.1 Constraints on Flattening of the Stellar Halo from B -magnitudes Alone

Fig. 2 shows how the observed faint star counts, taken from the MGC-BRIGHT catalogue, vary with Galactic longitude and magnitude. Also shown are the predicted counts from the model with a range of flattening of the stellar halo (the value of the axial ratio, (c/a), is given in parentheses in the Fig. 2, upper left). We quantified the fits of the models to the data as given in Table 1 and Fig 3, assuming that the errors on the counts are Poisson errors plus a maximum 3 per cent systematic error to be added in quadrature, derived from our estimates (see section 4 below) of the reliability of our stellar classification. In the range $17.0 < B_{\text{MGC}} < 19$ there is a consistent signal of a flattened halo, with axial ratio (c/a) ~ 0.5 , with the best fit giving an axial ratio of (c/a) = 0.54 ± 0.03 . In all cases the error given for the ratio (c/a) is the $\chi^2 + 1$ error (*i.e.*, 1σ). The rise for brighter magnitudes, where there are only ~ 30 stars in each field, is significant at only the $\sim 2\sigma$ level. The rise at fainter magnitudes may reflect real changes in the axial ratio with increasing Galactocentric radius (cf. Hartwick 1987) although the signal would have to be produced by intrinsically bright (and hence distant) tracers. Additionally, the presence of halo substructure could bias the result (see below, section 4.3).

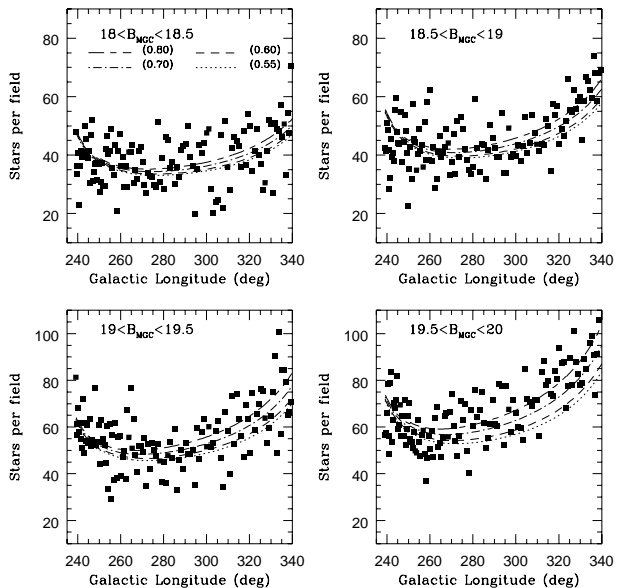


Figure 2. The MGC star counts as a function of Galactic longitude, in bins of apparent magnitude B_{MGC} , for $B_{\text{MGC}} > 18$ mag, compared to the predictions of star count models with a range of flattenings of the stellar halo. The axial ratio of the stellar halo is given in parentheses. Note here we have scaled the counts so that each field covers an area of 0.29 deg^2 .

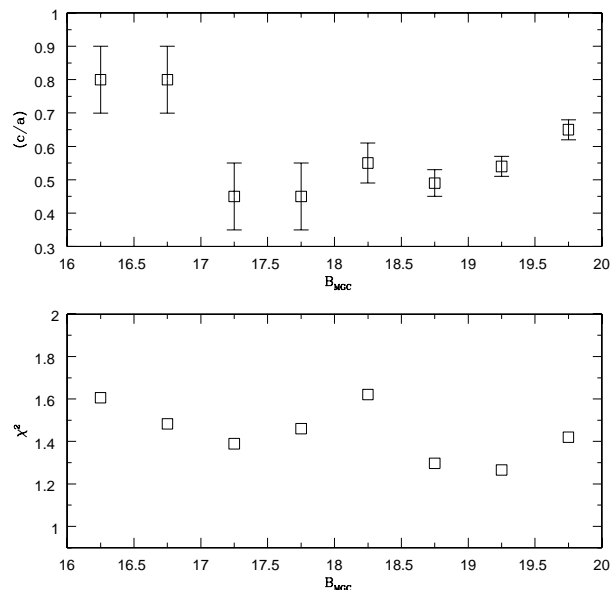


Figure 3. The quality of fit and axial ratio (c/a) of the best-fit star-count model in each magnitude bin from $16 < B_{\text{MGC}} < 20$. Here and throughout χ^2 refers to the minimum reduced χ^2 value. Also, unless otherwise indicated in the figure (through cuts in l and b), for each minimum χ^2 estimate there are 144 fields and hence 144 data points (see Fig. 2) and only one free parameter (the axial ratio of the stellar halo).

4.2 The Colour-Magnitude Diagram

Colour data for our star catalogue would allow us to identify particular spectral types of stars. The main sequence turn-off of the stellar halo is in the F-star region, and isolation of these stars maximizes the signal from the stellar halo, allowing a more sensitive testing of the flattening of the halo. Further, we can derive statistical measures of substructure in the stellar halo from analysis of the F-star distribution alone.

As noted above, the area covered by the MGC overlaps with part of the SDSS-EDR, specifically the SDSS run 756, stripe 10. We identified all the objects in the SDSS-EDR stellar database that lay within the MGC strip. Each object that was classified as a star in the MGC was then matched to the SDSS-EDR catalogue using a positional tolerance of $\Delta\theta = \pm 1$ arcsec (equivalent to ~ 3 pixels on the WFC camera). Of the 42413 MGC stars, 96.7 per cent had SDSS-EDR counterparts, and there was no case where an MGC star was matched to more than one SDSS-EDR star. Of the 1396 unmatched MGC stars, 49.79 per cent had $B_{\text{MGC}} < 15$, all of which fell in the “flooded stars region” of the B_{MGC} -Stellaricity plot (see Fig. 10 of Liske et al. 2003). This leaves a total of 41718 MGC-stars at $B_{\text{MGC}} > 16$ of which only 701 (2 per cent) have no SDSS-EDR counter-part. From these 701 unmatched objects, 115 were classified based on visual inspection by Liske, Lemon & Driver (Liske et al. 2003), and nearly all have $B_{\text{MGC}} > 19$. Of the remaining 586 stars, 151 fall into the known holes in the SDSS-EDR at $\sim 215.50^\circ < \text{RA} < 215.95^\circ$ and $\text{DEC} < -0.21^\circ$ and $0^\circ < \text{DEC} < 0.21^\circ$. A further 24 are clumped in a strip at $\sim 193.0^\circ < \text{RA} < 195.0^\circ$ and $0^\circ < \text{DEC} < 0.21^\circ$. The rest of the unmatched stars are evenly distributed across the MGC strip.

The SDSS-EDR magnitudes used in this paper are SDSS PSF magnitudes (see Lupton et al. 2003). Using the 41017 matched MGC-SDSS-EDR stars we are able to plot a colour-magnitude diagram (hereafter CMD; Fig. 4), and a colour-colour diagram (Fig. 5), for MGC stars in the range $16 < B_{\text{MGC}} < 20$. The $(B - V)$ colours are gained via the colour transformation found in Fukugita et al. (1996):

$$(g^* - r^*) = 1.05(B - V) - 0.23 \quad (1)$$

Three distinct concentrations of stars are obvious in the CMD of faint stars in high-latitude fields, representing the stellar halo, the thick disk and the thin disk, as shown in Gilmore & Wyse (1985; their Fig. 3) and in Gilmore et al. (1989; their Fig. 2). The first, seen here in Fig. 4 at $(B - V) \sim 0.45$, $B_{\text{MGC}} > 18$, reflects the main-sequence turnoff colour of metal-poor, old stars, and contains stars that are members of the stellar halo. The well-defined blue limit suggests a uniform old age for stars in the halo, with no significant intermediate-age population (see Unavane, Wyse & Gilmore 1996 for quantification of this point, and discussion of the implications for late accretion into the halo). The second concentration, at $(B - V) \sim 0.65$ and $B_{\text{MGC}} < 18$, marks the main-sequence turnoff of more metal-rich old stars, which reside in the thick disk (cf. Gilmore et al. 1985). The final concentration, at $(B - V) > 1.5$, is due to thin disk stars, and reflects the insensitivity of the B and V bands to cool stars on the main sequence (see Gilmore & Wyse 1987 for a comparison of the CMD in different band-passes). The

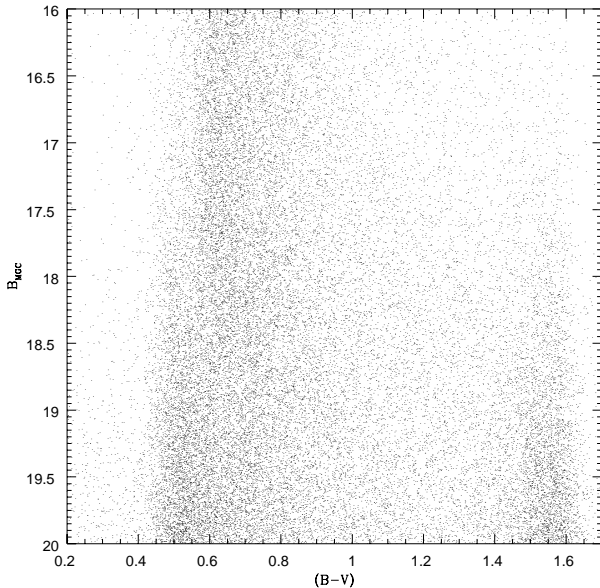


Figure 4. A CMD plot for the MGC stars in the range $16 < B_{\text{MGC}} < 20$.

CMD for the full SDSS-EDR data, in the SDSS band-passes, was presented by Chen et al. (2001) where the same features are seen.

It is clear from the morphology of the CMD that one cannot neglect the thick disk. It is also clear that the contribution of the stellar halo to our star counts is maximised by considering only F-stars, $B - V \lesssim 0.6$, and restricting the analysis to stars fainter than $B_{\text{MGC}} = 18$.

The colour-colour diagram of the MGC stars, using the SDSS photometry, is shown in Fig. 5 and provides a basis for spectral-type selection. Our chosen boundaries for various spectral classes of stars are as indicated. In principle F-stars cover a wide range in $(g^* - r^*)$ and $(u^* - g^*)$, but after taking into consideration the sharp halo turn-off at $(B - V) = 0.45$ (see Fig. 4 above), we adopted the more conservative limits $0.1 < (g^* - r^*) < 0.3$ and $0.7 < (u^* - g^*) < 1.0$ (see also Yanny et al. 2001, and Newberg et al. 2002 for similar selection criteria). The objects making up the fuzzy patch in the top left are likely to be quasars and contribute 2.5 per cent to the total MGC-SDSS matched sample. These should be distributed isotropically across the sky and so while increasing the background somewhat, should not contribute a false clustering or flattening signal.

4.3 Substructure in the Halo Star Counts

Hierarchical clustering scenarios of galaxy formation, such as in a Cold-Dark-Matter-dominated Universe, predict that the Milky Way formed from the merging of many smaller progenitors (see e.g. reviews of Silk & Wyse 1993 and White 1996). The satellite galaxies of the Milky Way may be surviving examples of the earlier systems. It has been suggested that a significant part of the *outer* halo could be the result of accretion and merging of substructure (cf. Searle & Zinn 1978), with this process on-going, as evidenced by the Sagittarius dwarf spheroidal (Ibata, Gilmore & Irwin 1994; Ibata

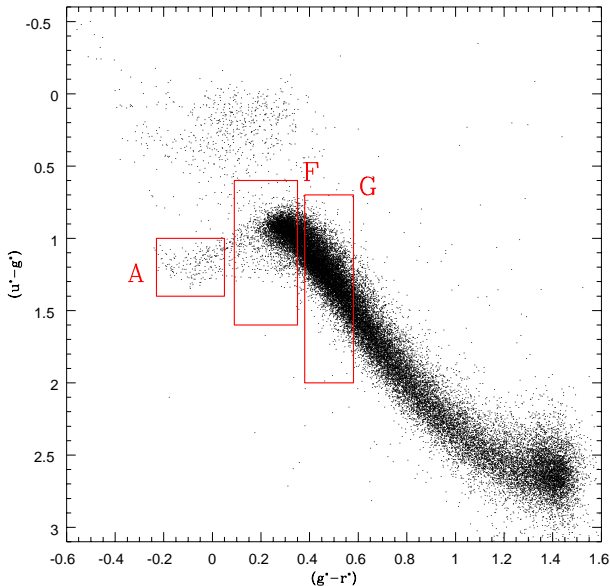


Figure 5. A colour-colour plot for the MGC stars in the range $16 < B_{MGC} < 20$. The boxes indicate the selection boundaries for A, F & G stars. Objects making up the fuzzy patch to the top left are most likely quasars.

et al. 1997). The kinematic signature of ‘moving groups’ is long-lived, producing observable effects at the solar Galactocentric distance and beyond, even after ~ 10 Gyr (Helmi & White 1999; Johnston et al. 1999; Helmi et al. 1999; Gilmore, Wyse & Norris 2002). The signature of clustering in coordinate space is less robust and decays faster in time with orbit wrapping, but has clearly been detected for the tidal streams from the Sagittarius dwarf spheroidal galaxy (Yanny et al. 2000; Vivas et al. 2001; Ibata et al. 2001, 2002). Newberg et al. (2002) identified several over-dense regions in their wide-area faint F-star sample using SDSS imaging data, several most likely to be associated with streams from the Sagittarius dwarf, but others that may be independent structures in the outer halo or disk. Indeed there may be a ‘ring’ around the Milky Way (Yanny et al. 2003; Ibata et al. 2003). These identified over-densities in the SDSS data are at faint magnitudes, $g^* \sim V > 19.4$, corresponding to $B_{MGC} \gtrsim 20$, or heliocentric distances of $\gtrsim 10$ kpc for metal-poor F-stars. Most of the mass of the stellar halo lies interior to these distances and is sampled by the brighter stars. Quantification of the level of substructure in these brighter stars (the inner halo) has heretofore been lacking in analyses of star counts.

Our present sample is ideal to quantify the clustering in the inner stellar halo, which contains the bulk of the stellar mass. This quantification of clustering has two applications, the first to constrain recent accretion, the second to estimate the possible effect of small-scale non-uniformities on our derivation of the larger-scale structure of the stellar halo. Simulations (e.g. Johnston et al. 1996) have shown that over-densities in coordinate space can survive for several orbital periods, albeit the alignment is dependent on the shape of the Galactic potential (longest for spherical potentials) and on the time dependence of the potential (e.g. Zhao

et al. 1999). The present analysis may be expected to constrain accretion into the inner halo over the last few Gyr, that being several orbital periods within several kpc of the Sun’s location. While the uniform old age of the bulk of the halo, seen again here in the location of the well-defined main sequence turn-off in Fig. 4, argues against the accretion of systems containing intermediate-age populations, such as the typical satellite galaxies, in the last ~ 10 Gyr being important in general (Unavane et al. 1996), the accretion of systems with stellar populations similar to the old, metal-poor halo is better constrained by signatures in kinematics and coordinate space.

4.3.1 Counts-in-Cells

A first impression of the clustering of the stars can be seen by a simple analysis of counts-in-cells. The contour and surface plots that results from counts in cells of size 0.1 degree in DEC and 5 degree in RA of the full MGC stellar distribution (irrespective of colour, and with limiting magnitude $B_{MGC} = 20$) is shown in Fig. 6 (note that there are around 10^3 stars per square degree at these magnitudes, with fields at high latitude and intermediate longitude, corresponding to the counts per cell here being around 500, and increasing towards the Galactic Center). The large scale gradient in the stellar distribution towards the direction of the Galactic Center is clearly seen. We removed this gradient by fitting a smooth quadratic to the stellar distribution in RA for each DEC bin, and then dividing the actual number of stars in each cell by the ‘model’ number of stars for that cell. In this way the large scale stellar distribution is taken out and only fluctuations due to random noise and/or stellar clustering are left, as shown in Fig. 7. Some fluctuations are seen in this plot, but all are at less than 1σ ($\sigma = 0.058$) away from the mean ($\frac{N}{N_{\text{model}}} = 1$).

Utilising colour information from the SDSS-EDR and isolating just the selected F-stars provides the contour and surface plots shown in Fig. 8; note that by restricting the colour range the number of stars per field has reduced to several tens rather than the several hundreds for all stars. Again fluctuations are seen, superimposed on the large scale gradient, but again at only low level of significance, at typical level of 1.27σ away from the mean.

The colour selection to narrow the spectral type also allows us to use apparent magnitude as an approximate distance modulus, since the selected F-stars should have a fairly narrow range in absolute magnitude. One can then look for clustering along the line-of-sight. The ‘pie-diagram’ plot of RA versus apparent magnitude (remember the survey is a narrow strip with little range in DEC) is shown in Fig. 9, with Fig. 10 showing the contour and surface plots in this RA- B_{MGC} plane. The rise in Fig. 10 shows the combination of the large scale stellar gradient and the stellar number count gradient, *i.e.*, more stars exist at fainter apparent magnitudes.

The strongest signal seen in our sample is again at the faintest magnitudes, $B_{MGC} \gtrsim 19$, and at larger RA $\gtrsim 210^\circ$; it is difficult to quantify the amplitude of the fluctuation due to the underlying increase in the star counts in both RA and apparent magnitude. As we will also see below, these values are close to the coordinates and apparent magnitude range

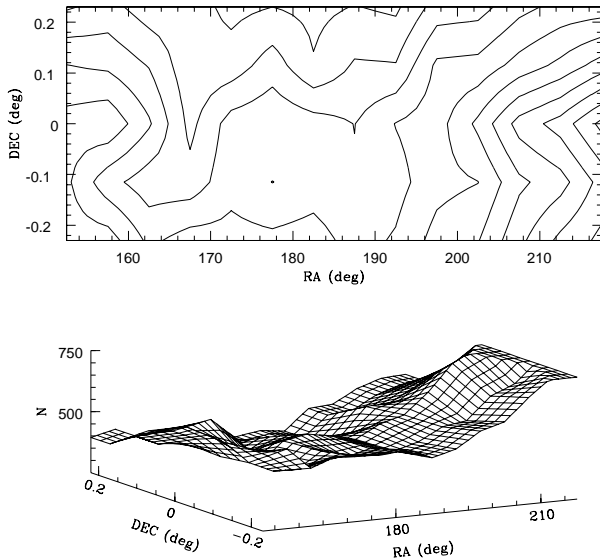


Figure 6. A contour (upper) and surface (lower) plot of the full stellar distribution. The large scale (galactic) stellar distribution is clearly visible. The contours are evenly spaced at intervals of $\Delta N=50$ between $N=300$ and $N=900$.

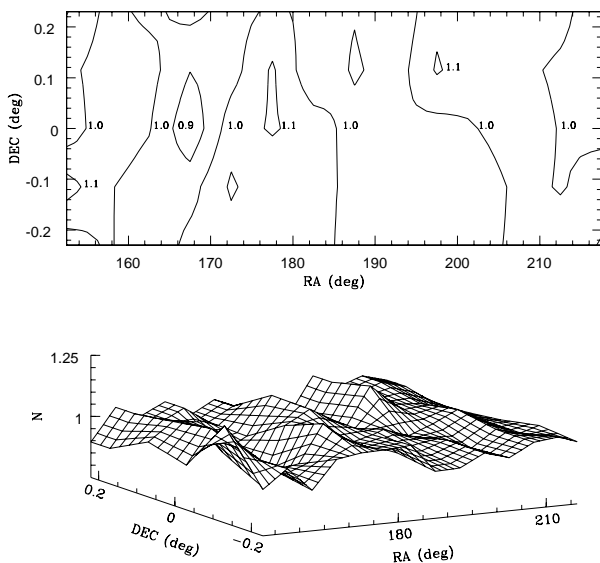


Figure 7. A contour (upper) and surface (lower) plot of the full “flat-fielded” stellar distribution with the large scale stellar distribution removed. The contours are evenly spaced at the levels of $\frac{N}{N_{\text{model}}}=0.9, 1.0$ and 1.1

of the detection of the tidal arm from the Sagittarius dwarf spheroidal galaxy in A-stars, at distances of ~ 40 kpc; this structure was identified in F-stars by Newberg et al. (2002), at apparent magnitudes of $g^* \sim 22.5$. That tidal feature represents material lost in the most pericentre passage of the Sagittarius dwarf, but tidal streams that were removed

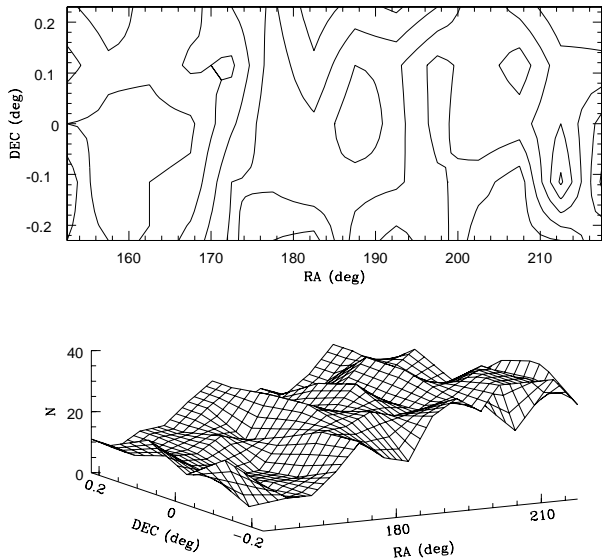


Figure 8. A contour (upper) and surface (lower) plot of the F-star distribution. The large scale (galactic) stellar distribution is clearly visible. The contours are evenly spaced at intervals of $\Delta N_F=5$ between $N_F=10$ and $N_F=60$.

1–2 pericentre passages ago are predicted in some models of the evolution of the Sagittarius dwarf (e.g. Johnston et al. 1999) to be seen in this direction at only 5–10 kpc from the Sun. The predictions are illustrated in Figure 4 of Kundu et al. (2002), who made a preliminary detection of this structure in bright K giant stars. The analysis of the 2MASS star counts by Majewski et al. (2003) also provides evidence of tidal debris from the Sagittarius dwarf in this location. While it is almost inevitable that there will be some contamination of the F-star data by stars of other spectral types, this should be relatively small since our colour cuts were conservatively chosen to minimise any contamination, and thus only random errors in colour should contribute. Thus we tentatively identify the apparent upwards fluctuation in counts with a tidal feature from the Sagittarius dwarf.

Further evidence of this feature’s reality comes from Fig. 11, which compares the projected spatial distributions of the F-stars and the full stellar samples, by taking the ratio of the star counts. Towards the end of the MGC strip there are bins in which the F-stars are more clustered. In other words, the surface plot in the lower panel of Fig 11 is not flat, which is what one might have expected if the F-stars were distributed in the same manner as the total stellar population. We now investigate other ways of quantifying this implied F-star clustering.

4.3.2 Angular correlation function

An alternative means of quantifying clustering on the sky is through the well-known angular correlation function, $\omega(\theta)$. This approach has been used widely to analyse the clustering properties of galaxies (e.g. Groth & Peebles 1977; Shanks et al. 1980; Maddox, Efstathiou & Sutherland 1996; Collins, Heydon-Dumbleton & MacGillivray 1989, Cabanac, de Lap-

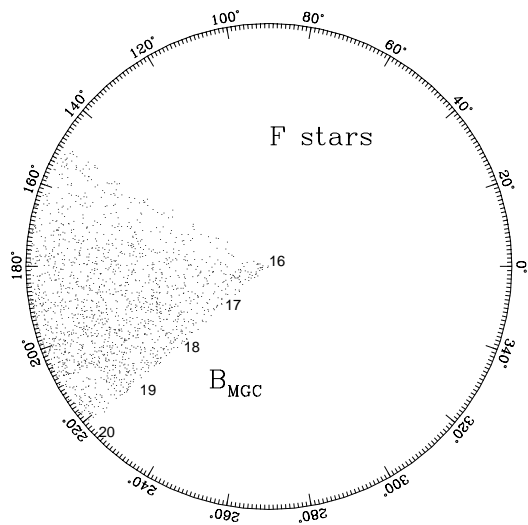


Figure 9. A ‘pie-diagram’ plot of RA and B_{MGC} for the F-star sample contained within the whole MGC b & l range.

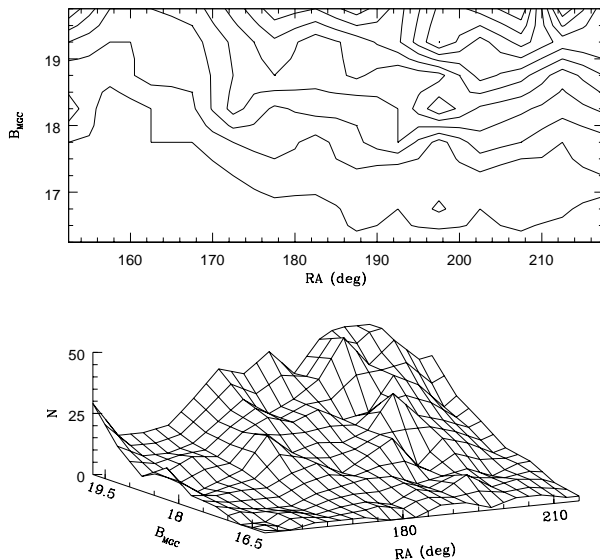


Figure 10. A contour and surface plot of the F-stars in RA-magnitude space. The contours are evenly spaced at intervals of $\Delta N=5$ between $N=10$ and $N=60$.

parent & Hickson 2000, Kümmel & Wagner 2000 and Couch, Jurcevic & Boyle 1993). Applications of the angular correlation function to samples of faint stars have been limited. Gilmore et al. (1985) derived the two-point correlation function of their large sample of faint, $B_J < 19.5$, Galactic stars, derived from photographic plates covering $\lesssim 30$ square degrees at high Galactic latitude, and showed that it was flat, consistent with a ‘complete absence of clustering’. These authors used this to argue that their star-galaxy separation was

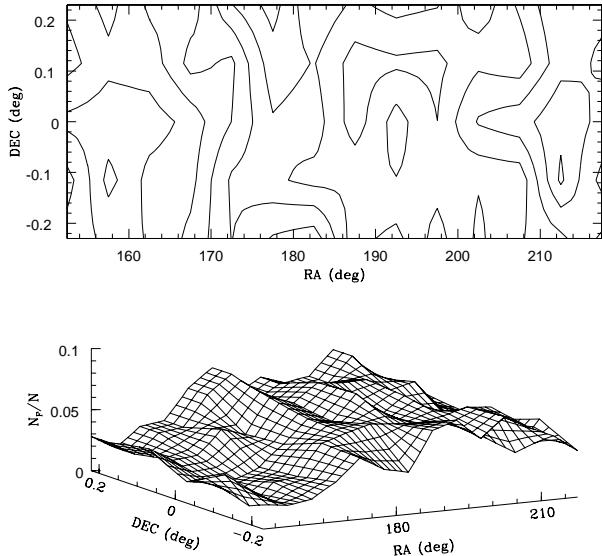


Figure 11. A contour (upper) and surface (lower) plots showing how the F-star distribution (N_F) compares to the full stellar distribution (N). The contours are evenly spaced at $\Delta \frac{N_F}{N}=0.01$ intervals between $\frac{N_F}{N}=0.01$ and $\frac{N_F}{N}=0.15$.

robust, and that patchy reddening was not important. They did not quantify what ‘complete absence’ meant in terms of limiting the existence of substructure. Doinidis & Beers (1989) analysed the angular correlation function of 4400 candidate field horizontal branch stars over 2300 square degrees, finding evidence for clustering on angular scales of $\lesssim 10''$, or physical scales of $\lesssim 25$ pc for the characteristic magnitude of the sample. They did not consider the clustering properties of more general field stars.

Here we want to quantify the (absence of?) features seen in the stellar angular correlation function. Of the different methods devised for measuring $\omega(\theta)$ we adopt the method used in Shanks et al. (1980) and Collins et al. (1989):

$$\omega(\theta) = \frac{N_{ss}}{N_{rr}} - 1 \quad (2)$$

Here N_{ss} is the number of star-star pairs with separation θ and N_{rr} is the number of simulated random-random pairs, again with separation θ . In practice we follow the same methodology as Doinidis & Beers (1989). In what follows, $\omega(\theta)$ will be derived from the mean random number of pairs calculated from 200 simulations. The simulations take into account the Galactic large scale stellar gradients and contain the same number of simulated stars as found in each sample. We calculate $\omega(\theta)$ for the range $0 < \theta < 5$ deg with $\Delta\theta=0.1^\circ$. Figs. 12, 13 & 14 display $\omega(\theta)$ as a function of θ for a bright F-star sample (limited brighter than $B_{\text{MGC}} = 19$), the full F-star sample, and the total MGC-SDSS matched stellar distributions respectively.²

The angular correlation functions are essentially flat,

² In order to save on computational time, for the total stellar distribution only 50 random simulations were used.

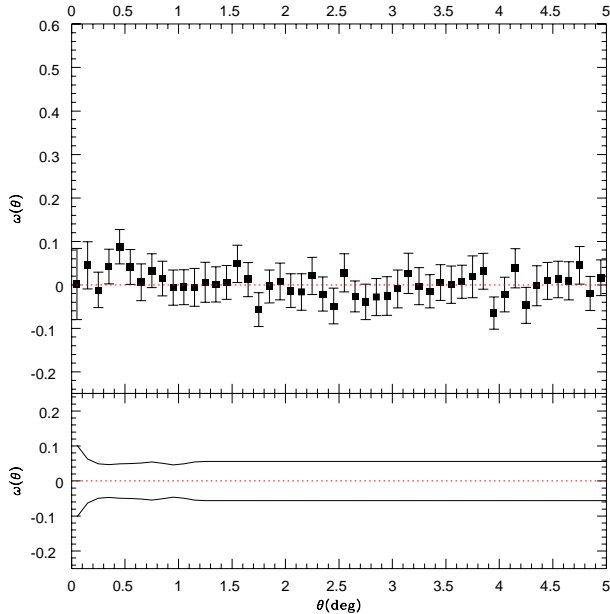


Figure 12. The upper panel shows the angular correlation function, $\omega(\theta)$, for the bright, $B_{\text{MGC}} < 19$, F-stars, as a function of angular separation, θ . The mean correlation function is shown by the dotted line and is flat and essentially zero. The errors shown are $\pm 1\sigma$ limits about the mean of each bin. No point is more than 3σ deviant. The lower panel shows the correlation functions of 200 random simulations, taking account of the overall gradient in stellar number density of the sample. The solid lines indicate the 1σ range of the simulations correlated about themselves; the fluctuations in the measured data correlation function are again seen to be at most about 3σ away from random.

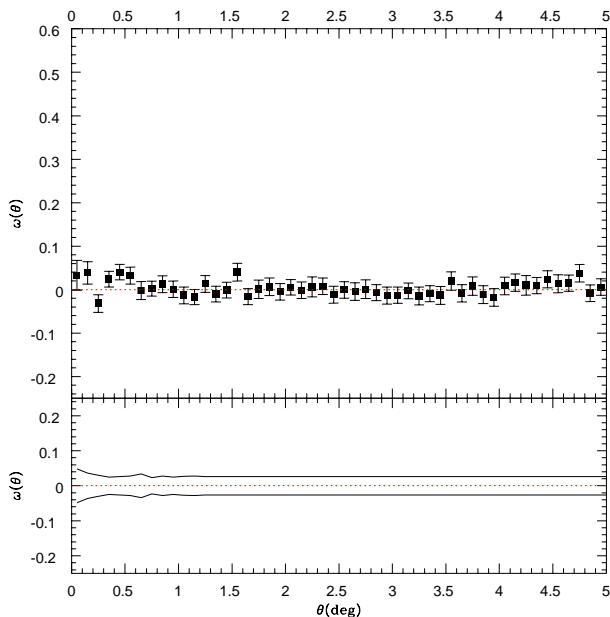


Figure 13. As Figure 12, but for all the F-stars, with no magnitude cut. Again the upper panel is the measured angular correlation function and the lower panel the results of random simulations. Again no deviations more significant than 3σ are seen.

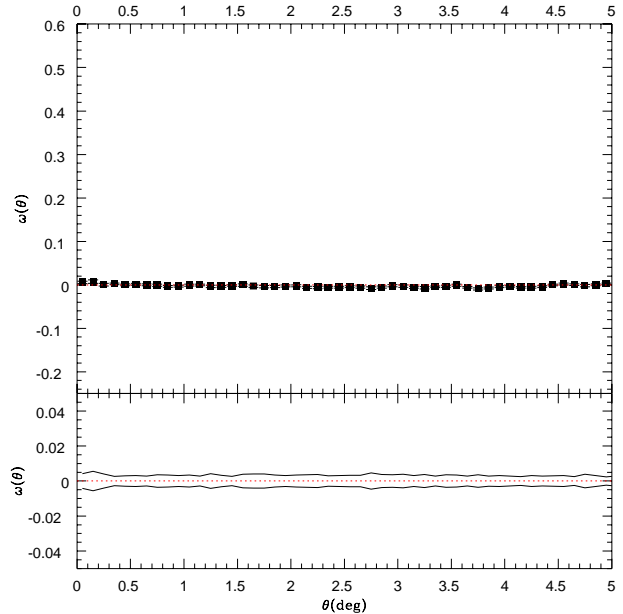


Figure 14. As Figure 12, but for the full MGC-SDSS matched stellar sample. Again the upper panel is the measured angular correlation function and the lower panel the results of random simulations. Again no deviations more than 3σ significant are seen.

with zero mean angular correlation function, fully consistent with a random distribution and no excess clustering at greater than the $3\text{-}\sigma$ level of significance. In Fig 13 $\omega(\theta)$ has both a mean and standard deviation of less than 0.005. The fluctuations detected may reflect simply statistics, as indicated by the variation seen in simulated random distributions, or may be in part attributable to patchy reddening/extinction (see Hewett 1983). To illustrate the spatial distribution of stellar colour in bins of size 0.2° by 0.1° is shown in Fig. 15 (limited to the first two degrees of the survey); although there is a mean of only 10 stars in each RA-DEC bin, the standard deviation in colour ($\sigma_{(u^*-g^*)}=0.2$) is significantly smaller than the mean standard deviation of colour across all bins ($\bar{\sigma}=0.6$). This uniformity of the colour indicates that the observed fluctuations are not due to random errors alone but that patchy reddening may contribute to the fluctuations on scales less than a degree.

Thus the angular two-point correlation function shows only barely significant clustering.

4.3.3 The Lee 2d statistic

The angular correlation function contains only low-level suggestion of any clustering, indeed limiting substructure to very low amplitude. The counts-in-cells did reveal substructure, but again at low significance. When examining just the F-stars and the F-star-all star ratio (see Figs 8 & 10 and 11) we have found that there are some small overdensities of faint stars towards the end of the MGC strip, which if real could be associated with tidal debris from previous pericentre passages of the Sagittarius dwarf. We now turn to more innovative tests for clustering, to see if they can either

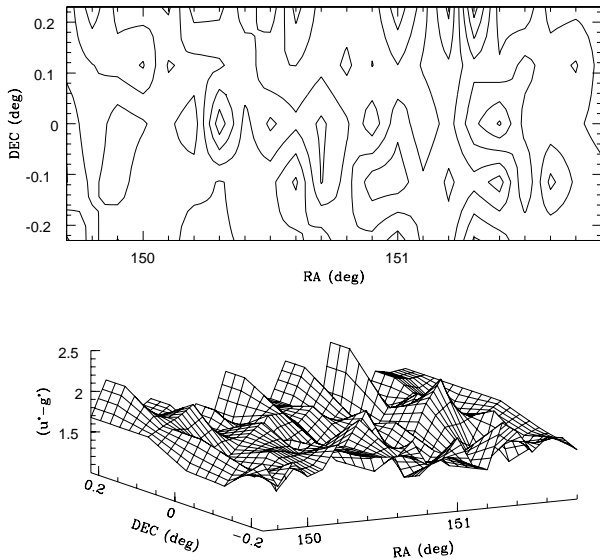


Figure 15. A contour (upper) and surface (lower) plot of the colour distribution in the first 2 degrees of the MGC strip. The contours mark the colour range $0.2 < (u^* - g^*) < 3$ in 0.2 intervals. The observed fluctuations have narrow colour ranges and are not thus probably not due to random effects alone (see text). This may reflect reddening that is patchy on scales of $\sim 1^\circ$.

place more stringent limitations, or indeed reveal low-level clustering with more significance.

The Lee 2d statistic (Lee 1979) has been used previously mostly in studies of substructure in clusters of galaxies, and indeed has been found to be the more sensitive test to the presence of structure (Rhee, van Haarlem & Katgert 1991) when compared to the angular separation test of West, Oemler & Dekel (1998; formally similar to the angular correlation function). A detailed discussion of the Lee statistic can be found in Fitchett (1988). The Lee 2d statistic is essentially a likelihood ratio, with the statistical analysis analogous to looking for the maximum likelihood split of a two-dimensional data set into two similar clumps.

The Lee statistic is calculated by projecting the data perpendicularly on to a line. At each point along this line a measure of the clumpiness of the data is found and a maximum determined, $L(\theta)$. The clumpiness is determined at each point/partition along the line by measuring the deviation away from the mean (or Gaussian distribution) of all the points to the left and right of the partition. This is then compared to the deviation away from the mean of the total data set. In this way any underlying large-scale structure gradient is “flat fielded” out as part of the analysis process. The line is then rotated by some small amount, $\Delta\theta$, and the process is repeated. From this we can plot $L(\theta)$ against θ , the maximum of which, $L(\theta)_{\max}$, indicates the position angle of a line partitioning the data into two clumps. The Lee 2d statistic has been used to look for substructure within galaxies, clusters of galaxies (Fitchett & Webster 1987; Rhee et al. 1991) and in simulations of clusters (Crone, Evrard & Richstone 1996). We now apply it to our high-latitude stellar data set.

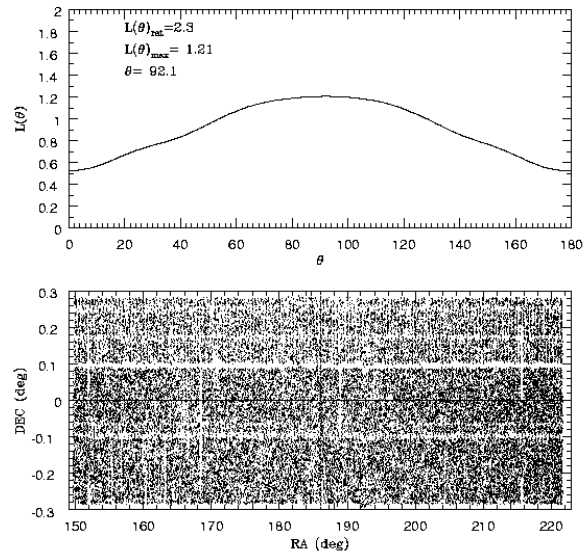


Figure 16. Upper: A plot of $L(\theta)_{\max}$ for the high latitude stellar sample. Lower: The full MGC-SDSS stellar sample on the sky.

We first apply this test to the (projected) angular distribution on the sky of the entire MGC-SDSS matched stellar data set. The data are shown in the lower panel of Fig. 16 and the values of the Lee statistic $L(\theta)$ for this sample are shown in the upper panel. The position angle, θ_{\max} , of the maximum of the Lee statistic is indicated in the lower panel.

The $L(\theta)$ curve shows a rather broad peak, indicating only a low-significance detection of an over-density; a stronger detection would result in a more obvious peak. The value of the angle at which the Lee statistic has its maximum, $\theta_{\max} = 92.1$, indicates that the overdensity is located towards the top right of the lower plot, again at high values of RA (as in the earlier statistical tests). The significance of this detection can be quantified by the analysis of randomly distributed datasets. Thus we fill the MGC survey area with the same number of stars as found in the high latitude sample, but randomly distributed (remember that any large-scale gradient is removed by the analysis technique). Fig. 17 shows the simulated dataset, as well as the corresponding $L(\theta)$ plot. The angle at which $L(\theta)_{\max}$ occurs is now 90.7° , the slight offset from the perpendicular being understandable as due to the uneven distribution of MGC exclusion regions.

We note that for the simulated data the L_{rat} statistic is higher, indicating a more significant detection (of the MGC holes), than in the real data. This can be explained by noting that in the simulations there was no minimum star-star separation used. Therefore the simulated stellar distribution will be slightly smoother than the real data, making

the effects of the MGC holes more apparent in the simulation. This implies that any result from the Lee 2d test will provide only a rough estimate on the size of the clustering signal. The lack of a minimum star-star separation in the simulated data should not have affected the $\omega(\theta)$ test as it is only dependent on the number of stars at a given radius and not their distribution about a partition.

Taking the ratio of $L(\theta)_{rat} \left(= \frac{L(\theta)_{max}}{L(\theta)_{min}} \right)$ for the simulated and real data we find that the over-density seen in the MGC region is detected at 8 per cent $\left(= 100 \times \text{mod} \left(1 - \frac{L(\theta)_{rat_{MGC}}}{L(\theta)_{rat_{MGC_{sim}}} \right) \right)$ above a smooth stellar distribution.

To summarise the Lee 2d scheme, a line at some angle, θ , is drawn dividing the data in half. Every star is then projected onto that line, defining a partition point for each star. The clumpiness/asymmetry parameter $L(\theta)$ is then calculated for all stars/partitions along the line and the largest value of $L(\theta)$ is found for that line/angle. The MGC RA and DEC coordinates of the star whose partition gave that value of $L(\theta)$ is then used as the coordinates of the over-density. By doing this for the entire stellar sample from the MGC, we find a weak clustering signal at RA=216.5° and DEC=0°, consistent with visual inspection of the distribution of the stars. This is consistent with the counts-in-cells analysis, and again if real can be a combination of A-stars from the distant, most recent, tidal debris from the Sagittarius dwarf (cf. Yanny et al. 2000; Vivas et al. 2001; Ibata et al. 2001), and F-stars from an older, more nearby, tidal stream.

Having shown that the Lee 2d statistic is sensitive to substructure, we now investigate the signal for the inner halo by using only the brighter F-stars, in the magnitude range $17.5 < B_{MGC} < 19$. Figs. 18 and 19 show the results of the Lee 2d test for the real and simulated (random distribution) F-star population. We find a slightly stronger clustering signal by isolating F-stars, with an amplitude of 14 per cent deviation from a random distribution, with the clustering now placed at RA=205° and DEC=0°. Again this places it within the 2-D coordinate space covered by a Sagittarius dwarf tidal stream, with the inferred distances (if F-stars and not A-star contamination) pointing to debris from an older pericentre passage (Johnston et al. 1999). We find no other evidence of clustering.

4.4 Halo Flattening Revisited

Although there is no strong detection of structure within the Galactic halo sampled, we decided, to be conservative, to re-fit the star-count models to a restricted sub-sample. We now fit to star count data at $b > 45^\circ$ and for data in the range $b > 45^\circ$ and $l < 340^\circ$ (see Tables 2 & 3). This was done to minimize the contributions from the thin/thick disks and the thin/thick disks and bulge respectively. Note that this longitude cut also serves to remove any effects of the Sagittarius Dwarf tidal stream. Fig. 20 shows the effect of removing the low latitude and high longitude fields from the χ^2 fitting; a stellar halo with an axial ratio of $(c/a)=0.52 \pm 0.05$ now provides the best fit to the data. The sample is dominated by stars within ~ 10 kpc of the Sun, and this axial ratio thus applies to the inner halo.

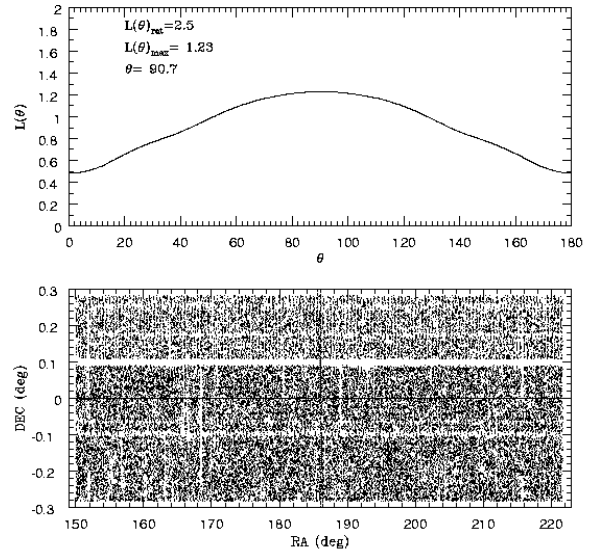


Figure 17. Upper: A plot of $L(\theta)_{max}$ for the simulated high latitude stellar sample. Lower: The full simulated stellar sample.

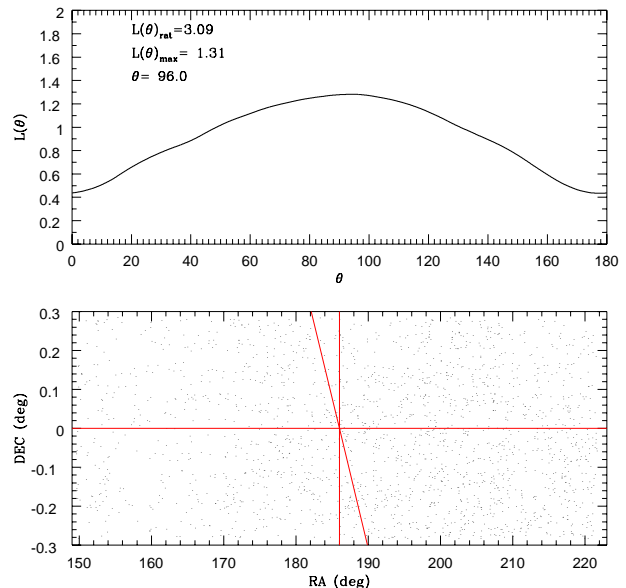


Figure 18. The Lee 2d test for the F-star sample. The upper and lower panels are the same as in Fig. 16.

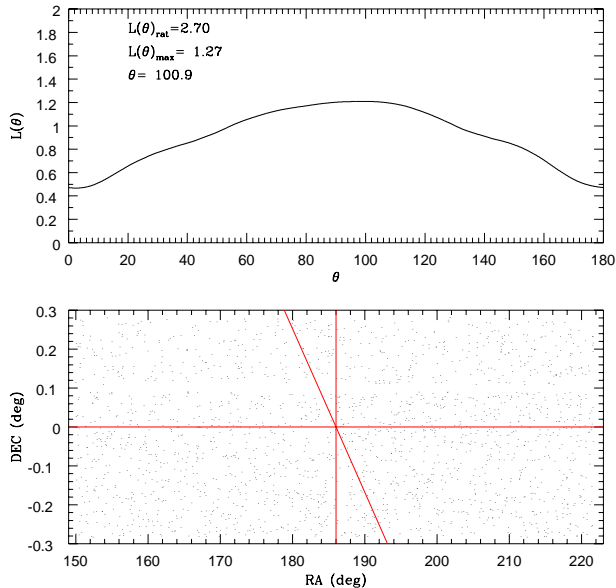


Figure 19. The Lee 2d test for the simulated F-star sample. The upper and lower panels are the same as in Fig. 17.

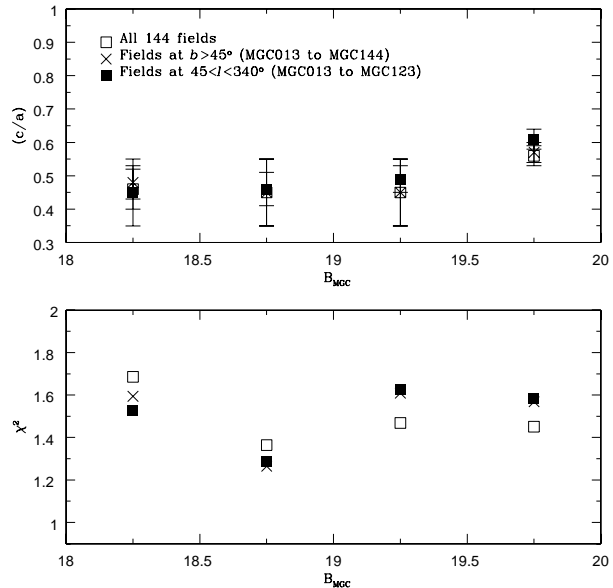


Figure 21. Here we show the effects of using a potentially cleaner sample, one consisting of only MGC-SDSS matched stars with $(u^* - g^*) > 0.6$.

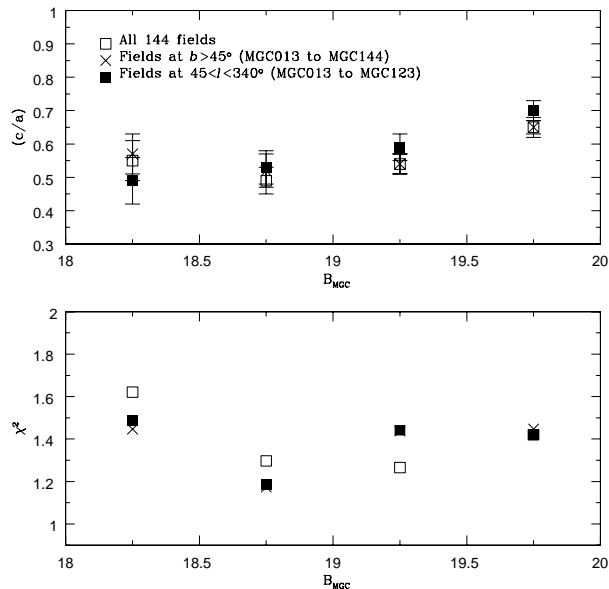


Figure 20. Here we show the effect on the favored axial ratio of the stellar halo of removing the low ($b < 45^\circ$) Galactic latitude and high ($l > 340^\circ$) Galactic longitude fields from the χ^2 fitting.

A further refined sample contains only MGC-SDSS matched stars with $(u^* - g^*) > 0.6$. Although there are 2418 fewer stars in this subsample than in the full stellar sample 1021 of the rejected stars having $(u^* - g^*) < 0.6$, this sub-sample should now be free from any spurious effect that may have been induced by the possible inclusion of QSOs (previously identified as the fuzzy patch in Fig. 5).

Table 4 shows the best fit halo axial ratio in each magnitude bin for the sample with Galactic latitude and longitude

cuts, and Fig. 21 compares the results from this reduced sample to the original one. In fact the χ^2 values and overall shape of the “axial-profile” remain more or less the same. It is only the value of the halo axial-ratio that has changed, with the reduced sample preferring a slightly more flattened halo, with $(c/a) = 0.45 \pm 0.1$. Note that as the models are only generated within the range $0.45 \leq (c/a) \leq 0.8$, any ‘best-fit’ model with an axial ratio less than 0.45 is spurious and simply represents a lack of stars within the magnitude bin and b and l range being tested.

The star-count models are then fitted to the full MGC stellar sample, to the MGC-SDSS sample (i.e. no colour cuts) and to the F-star sample in the magnitude range $18 < B_{\text{MGC}} < 19$, both with and without the b and l cuts. In doing this we find that the best fit comes from the full MGC stellar sample with both the b and l cuts and gives an axial ratio of $(c/a) = 0.61 \pm 0.02$. However, the axial ratio with the smallest error is given by the F-star sample, again with both the b and l cuts, $(c/a) = 0.56 \pm 0.01$. This is again sampling the inner halo.

In comparing our results with previous work we find that our final value is in very good agreement with the pioneering work of Kinman, Wirtanen & Janes (1965) who reported $(c/a) = 0.6$ for the stellar halo interior to the Sun, based on a small (less than 100) sample of bright RR Lyrae stars. Indeed most star-count analyses of the inner halo give a flattening of this order (e.g. Hartwick 1987; Wyse & Gilmore 1989; Larsen & Humphreys 1994, 2003; Siegel et al. 2002), consistent with anisotropic velocity dispersions (Wyse & Gilmore 1989; Chiba & Beers 2000). The outer stellar halo may be rounder (e.g. Hartwick 1987; Preston, Shtetman & Beers 1991), perhaps reflecting a differing importance of dissipation during formation of the inner and outer halo (cf. Norris 1994; Chiba & Beers 2001). A detailed investigation of the variation of flattening with distance is

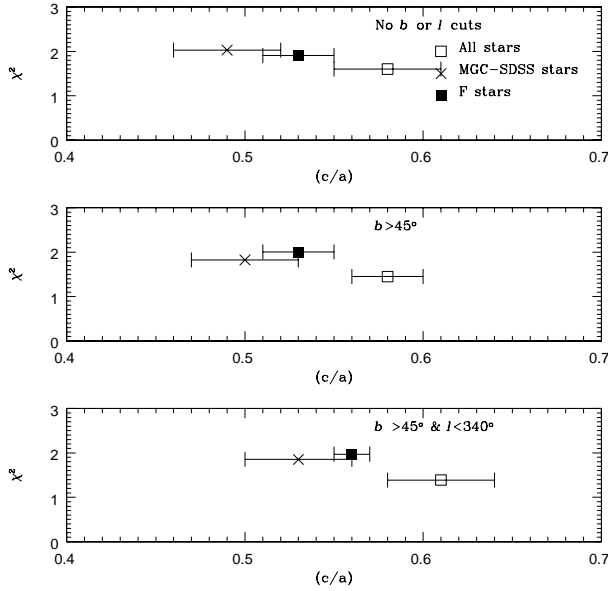


Figure 22. A graphical summary of all the best fit star-count models for each stellar sample.

beyond the scope of the limited data given here, but well within the scope of the final SDSS dataset. However we do note that our more local F-star analysis yields a marginally significantly lower (c/a) than the full stellar population. Furthermore we note that within our analysis we see a marginal increase in (c/a) with magnitude (distance), (Fig. 3, 20, & 21), however this could also be explained by contamination from the QSO and/or galaxy population at the star-galaxy separation limit.

5 CONCLUSIONS

We have used a sample of 42457 stars from the MGC-Bright photometric catalogue, most of which (~ 97 per cent) have SDSS-EDR counterparts, to investigate the structure of the stellar halo of the Milky Way. The MGC-SDSS matched objects were used to define colour selection limits allowing us to isolate a sample of F-stars. Our major results are the first quantification of the clustering in coordinate space in the inner halo, plus a new estimate of the large-scale flattening of the inner halo.

We conclude that the stellar halo of the Milky Way is significantly flattened, with an axial ratio of $(c/a)=0.56\pm 0.01$ (within $R \leq 10$ kpc). While this result is in line with previous determinations, it is more robust, having been derived from samples cleaned of substructure and with contamination from quasars and other stellar components minimised.

We find weak evidence for substructure in the brighter F-stars, tentatively identified with tidal debris from the Sagittarius dwarf. We find no other substructure. This essentially null result implies that recent accretion of stellar systems is not important in the bulk of the stellar halo. Quantification of limits on the disruption rate of putative satellites needs to be investigated, but is beyond the scope

of the present paper. However these firm limits of observable clustering need to be included in future hierarchical clustering models.

We thank Gerry Gilmore for updated star-count models. RFGW acknowledges receipt of a Visiting Fellowship from PPARC and thanks all for a stimulating and pleasant environment during her sabbatical.

REFERENCES

- Bahcall J.N., Soneira R., 1984, *ApJS*, 55, 67
 Bertin E., Arnouts S., 1996, *A&AS*, 117, 393
 Buser, R., Rong, J., Karaali, S., 1999, *A & A*, 348, 98
 Cabanac R.A., de Lapparent V., Hickson P., 2000, *A&A*, 364, 349
 Chen B. et al., 2001, *ApJ*, 553, 184
 Chiba, M., Beers, T.C., 2001, *ApJ*, 549, 325
 Chiba, M., Beers, T.C., 2000, *AJ*, 119, 2843
 Collins C.A., Heydon-Dumbleton N.H., MacGillivray H.T., 1989, *MNRAS*, 236, 7
 Colless M. et al., 2001, *MNRAS*, 328, 1039
 Couch W.J., Jurcevic J.S., Boyle B.J., 1993, *MNRAS*, 260, 241
 Crone M.C., Evrard A.E., Richstone D.O., 1996, *ApJ*, 467, 489
 Doinidis S.P., Beers T.C., 1989, *ApJ*, 340, 57
 Elvius, T. 1965, in ‘Galactic Structure’, eds A. Blaauw & M. Schmidt (Univ of Chicago Press, Chicago), chapter 3
 Fitchett M., 1988, *MNRAS*, 230, 161
 Fitchett M., Webster R., 1987, *ApJ*, 317, 653
 Fukugita M., Ichikawa T., Gunn J.E., Doi M., Shimasaku k., Schneider D.P., 1996, *AJ*, 111, 1748
 Gilmore G., 1984, *MNRAS*, 207, 223
 Gilmore G., Reid I.N., 1983, *MNRAS*, 202, 1025
 Gilmore G., Wyse R.F.G., 1985, *AJ*, 90, 10
 Gilmore G., Wyse R.F.G., 1987, in ‘The Galaxy’, eds G. Gilmore and B. Carswell, Reidel, Dordrecht, p247
 Gilmore G., Reid I.N., Hewett P., 1985, *MNRAS*, 213, 257
 Gilmore G., Wyse R.F.G., Kuijken K., 1989, *ARA&A*, 27, 555
 Gilmore G., Wyse R.F.G., Jones J.B., 1995, *AJ*, 109, 1095
 Gilmore G., Wyse R.F.G., Norris J., 2002, *ApJ*, 574, L39
 Groth E., Peebles P.J.E., 1997, *ApJ*, 217, 385
 Hartwick F.D.A., 1987, in ‘The Galaxy’, eds G. Gilmore and B. Carswell, Reidel, Dordrecht, p281
 Helmi A., White S.D.M., 1999, *MNRAS*, 307, 495
 Helmi A., White S.D.M., de Zeeuw P.T., Zhao H.-S., 1999, *Nature*, 402, 53
 Hewett, P.C., 1983, PhD thesis, Univ. Edinburgh
 Ibata R., Gilmore G., Irwin M., 1994, *Nature*, 370, 194
 Ibata R., Wyse R.F.G., Gilmore G., Irwin M., Suntzeff N., 1997, *AJ*, 113, 634
 Ibata R., Irwin M., Lewis G.F., Stolte A., 2001, *ApJ*, 547, L133
 Ibata R., Lewis G.F., Irwin M., Cambresy L., 2002, *MNRAS*, 332, 921
 Ibata R., Irwin M., Lewis G.F., Ferguson, A. & Tanvir, N., 2003, *MNRAS*, 340, L21
 Johnston K.V., Hernquist L., Bolte M., 1996, *ApJ*, 465, 278
 Johnston K.V., Majewski S., Siegel M., Reid I.N., Kunkel W., 1999, *AJ*, 118, 1719
 Kinman, T.D., Wirtanen, C.A. & Janes, K.A. 1965, *ApJS*, 11, 223
 Kümmel M.W., Wagner S.J., 2000, *A&A*, 353, 867
 Kundu, A., et al. 2002, *ApJ*, 576, L125
 Larsen, J.A., Humphreys, R.M., 1994, *ApJ*, 436, L149
 Larsen, J.A., Humphreys, R.M., 2003, *AJ*, 125, 1958
 Lee K.L., 1979, *J. Am. statist. Ass*, 74, No. 367, 708
 Liske J., Lemon D.J., Driver S., Cross N.J.G., Couch W.J., 2003, *MNRAS*, submitted
 Lupton R.H. et al., 2003, in preparation

- Maddox S.J., Efstathiou G., Sutherland W.J., 1996, MNRAS, 283, 1227
- Majewski, S., Skrutskie, M., Weinberg, M. & Ostheimer, J. 2003, ApJ submitted (astro-ph/0304198)
- Morrison H., 1993, AJ, 106, 578
- Newberg H. et al., 2002, ApJ, 569, 245
- Ng, Y.K., Bertelli, G., Chiosi, C., Bressan, A., 1997, A & A, 324, 65
- Norris J.E. 1994, ApJ, 431, 645
- Norris J.E., Ryan S., 1991, ApJ, 380, 403
- Oort, J. 1958, in Stellar Populations eds D. O'Connell (North Holland, Amsterdam) p507
- Preston, G.W., Schectman, S.A., Beers, T.C., 1991, ApJ, 375, 121
- Reid I.N., Majewski S., 1993, ApJ, 409, 635
- Reylé, C. & Robin, A.C. 2001, A & A, 373, 886
- Rhee G.F.R.N., van Haarlem M.P., Katgert P., 1991, A&A 246, 301
- Searle L., Zinn R., 1978, ApJ, 225, 3575
- Shanks T., Fong R., Ellis R.S., 1980, MNRAS, 192, 209
- Siegel, M.H., Majewski, S.R., Reid, I.N., Thompson, I.B., 2002, ApJ, 578, 151
- Silk J., Wyse R.F.G., 1993, Phys. Rep. 231, 295
- Stoughton C. et al., 2002, AJ, 123, 485
- Unavane M., Wyse R.F.G., Gilmore G., 1996, MNRAS, 278, 727
- Vivas A.K. et al., 2001, ApJ, 554, L33
- West M., Oemler Jr. A., Dekel A., 1998, 327, 1
- White S.D.M., 1985, ApJL, 294, L99
- White S.D.M., 1996, in 'Cosmology & Large Scale Structure', Les Houches Session LX, eds R. Schaeffer, J. Silk, M. Spiro, J. Zinn-Justin, Elsevier, Amsterdam, p349
- Wielen R., 1974, in Highlights of Astronomy, Vol 3, ed. G. Contopoulos, Dordrecht: D. Reidel, p. 395
- Wyse R.F.G., Gilmore G., 1989, Comments on Astronomy, 13:3, 135
- Yanny B. et al., 2000, AJ, 540, 825
- Yanny B. et al., 2003, ApJ, 588, 824
- York D.G. et al., 2000, AJ, 120, 1579
- Yoshii, Y., 1982, PASJ, 34, 365
- Zhang B., Wyse R.F.G., Stiavelli M., Silk J., 2002, MNRAS, 332, 647
- Zhao H.-S., Johnston K.V., Hernquist L., Spergel D.N., 1999, A&A, 348, 49

TABLES

Table 1. The best fit model in each magnitude bin using all the data.

B_{MGC}	(c/a)	χ^2
$18.0 < B_{\text{MGC}} < 18.5$	0.55 ± 0.06	1.62
$18.5 < B_{\text{MGC}} < 19.0$	0.49 ± 0.04	1.30
$19.0 < B_{\text{MGC}} < 19.5$	0.54 ± 0.03	1.27
$19.5 < B_{\text{MGC}} < 20.0$	0.65 ± 0.03	1.42

Table 2. The best fit model in each magnitude bin using all data at $b > 45^\circ$.

B_{MGC}	(c/a)	χ^2
$18.0 < B_{\text{MGC}} < 18.5$	0.57 ± 0.06	1.45
$18.5 < B_{\text{MGC}} < 19.0$	0.52 ± 0.05	1.17
$19.0 < B_{\text{MGC}} < 19.5$	0.54 ± 0.04	1.44
$19.5 < B_{\text{MGC}} < 20.0$	0.65 ± 0.04	1.45

Table 3. The best model in each magnitude bin in using all data at $b > 45^\circ$ & $l < 340^\circ$.

B_{MGC}	(c/a)	χ^2
$18.0 < B_{\text{MGC}} < 18.5$	0.49 ± 0.08	1.49
$18.5 < B_{\text{MGC}} < 19.0$	0.53 ± 0.06	1.18
$19.0 < B_{\text{MGC}} < 19.5$	0.59 ± 0.04	1.44
$19.5 < B_{\text{MGC}} < 20.0$	0.70 ± 0.03	1.45

Table 4. The best model in each magnitude bin using colour selected stars, with $(u^* - g^*) > 0.6$, at $b > 45^\circ$ & $l < 340^\circ$.

B_{MGC}	(c/a)	χ^2
$18.0 < B_{\text{MGC}} < 18.5$	0.45 ± 0.10	1.53
$18.5 < B_{\text{MGC}} < 19.0$	0.46 ± 0.10	1.28
$19.0 < B_{\text{MGC}} < 19.5$	0.49 ± 0.06	1.62
$19.5 < B_{\text{MGC}} < 20.0$	0.61 ± 0.04	1.58